

## Stabilization of Catanionic Vesicles via Polymerization

Zhiyuan Zhu,<sup>†,‡</sup> Hangxun Xu,<sup>†,‡</sup> Hewen Liu,<sup>†</sup> Yamaira I. González,<sup>§</sup> Eric W. Kaler,<sup>§</sup> and Shiyong Liu<sup>\*,†,‡</sup>

Department of Polymer Science and Engineering, University of Science and Technology of China, Hefei, 230026, Anhui Province, P.R. China, The Hefei National Laboratory for Physical Sciences at Microscale, Hefei, 230026 Anhui Province, P. R. China, and Department of Chemical Engineering, University of Delaware, Newark, Delaware 19716, USA

Received: January 25, 2006; In Final Form: June 5, 2006

Polymerizable cationic surfactant methacryloyloxyoctyl trimethylammonium bromide (MOTB) and anionic surfactant sodium 4-( $\omega$ -methacryloyloxyoctyl)oxy benzene sulfonate (MOBS) were synthesized. Stable catanionic vesicles can spontaneously form upon mixing the two oppositely charged surfactants in aqueous solution, which was further permanently fixed by polymerization. Surface tensiometry, nuclear magnetic resonance (NMR), static and dynamic laser light scattering (LLS), and cryogenic transmission electron microscopy (cryo-TEM) were used in combination to characterize the catanionic vesicles before and after polymerization. The kinetics of formation and breakdown of unpolymerized catanionic vesicles were studied in detail employing stopped-flow light scattering. In contrast to unpolymerized vesicles, the polymerized ones exhibit permanent stability under external perturbations such as dilution or adding excess MOTB. A tentative explanation is proposed about why free radical polymerization can successfully fix the catanionic vesicles, the structure of which is well-known to be in dynamic equilibrium exchange with unimers.

### Introduction

Aqueous mixtures of single-tailed cationic and anionic surfactants (catanionics) can produce a large variety of morphologically different aggregate microstructures, such as spherical and rodlike micelles, vesicles, lamellar phases, and even precipitate.<sup>1–9</sup> Their structural resemblance to primitive biological cells makes vesicle phases useful as biological membrane models, drug delivery vehicles, or nanocompartments for the formation of biomaterials.<sup>1,10,11</sup> Most importantly, catanionic vesicles with well-controlled size, surface charge, and permeability can spontaneously form by mixing commercially available single chain surfactants.<sup>3,4,12</sup>

The thermodynamics of the formation of catanionic vesicles has received detailed investigations. Some catanionic vesicles reach equilibrium in  $\sim 3$  months, and after this time, no further change is observed.<sup>3,4</sup> They are infinitely stable if the solution conditions are kept unchanged. However, a small variation in the intermolecular force balance (pH, ionic strength, temperature, dilution, organic solvent, etc.) may induce a reorganization of the surfactant molecules leading to phase separation or structural transition.<sup>9,13–20</sup> Although the steady state of the vesicle phases is now well-characterized, much less is known about the kinetics of spontaneous vesicle formation and their microstructural reorganization under variation of external conditions.<sup>12–14,20–24</sup> The knowledge of the latter is not only of scientific interest but plays an important role in real-world applications where vesicles are envisioned.<sup>25–28</sup>

Hatton et al. studied the kinetics of formation of catanionic vesicles from sodium octyl sulfate (SOS)/cetyltrimethylammo-

nium bromide (CTAB) or sodium dodecyl sulfate (SDS)/dodecyltrimethylammonium bromide (DTAB).<sup>21,23</sup> The vesicle formation process is believed to be composed of a sequence of four steps, immediately after stopped-flow mixing the two surfactants. The first step, which is fast (completed within the stopped-flow “dead” time of  $\sim 4$  ms), is associated with the formation of nonequilibrium mixed aggregates. This step is followed by the formation of loose or “floppy” bilayer structures through rearrangement of nonequilibrium mixed aggregates ( $\sim 4$  s). The two remaining steps include formation of vesicle precursors ( $\sim 100$  s) and formation of the final equilibrium vesicles ( $\sim 2000$  s).

Gradzielski et al. also studied the kinetics of vesicle formation from equimolar mixtures of the anionic surfactant, Texapon N<sub>70</sub>-H, and cationic surfactant, tetradecyltrimethylammonium hydroxide using a combination of stopped-flow and small-angle X-ray scattering (SAXS).<sup>24</sup> Their results confirm that vesicle formation is a complex multistep process, with the initial formation of mixed globular micelles, followed by the quick formation of floppy bilayers. The bilayers then close in a much slower process and form unilamellar vesicles. It should be noted that the kinetics of catanionic vesicle formation is system-dependent. For SOS/CTAB system, it takes months to relax into the final equilibrium vesicles, whereas for dodecyl benzene sulfonic acid (HDBS)/CTAB system, the vesicle formation is completed within minutes.<sup>20</sup> Thus it is imperative to investigate more catanionic vesicle systems so that general guidelines of their kinetics of formation may hopefully be established.

As compared with that of vesicle formation, the kinetics of vesicle breakdown upon dilution, addition of excess of single chain surfactant or organic solvent (toluene) is even less studied.<sup>16,21,22</sup> An understanding of the kinetics of vesicle breakdown is relevant for those applications in which vesicle stability is crucial. For SOS/CTAB or SDS/DTAB catanionic

\* Corresponding author phone: 0086 551 3607348; fax: 0086 551 3607348; e-mail: sliu@ustc.edu.cn.

<sup>†</sup> University of Science and Technology of China.

<sup>‡</sup> The Hefei National Laboratory for Physical Sciences at Microscale.

<sup>§</sup> University of Delaware.

vesicles, Hatton et al. reported that the vesicle breakdown upon addition of excess SOS or SDS appeared to be a rapid single-step process, with time constants smaller than 4 ms for SOS/CTAB and  $\sim 10$  s for SDS/DTAB vesicles.<sup>21</sup> Additional work by Robinson et al. showed that the breakdown of SOS/CTAB vesicles linearly depended on the concentration of the added single-chain surfactant.<sup>22</sup>

The instability of catanionic vesicles and other self-assembled structures upon changes in solution conditions has also prompted our continual studies on the structural fixation of these nanostructures made of surfactants and amphiphilic block copolymers.<sup>29–35</sup> The covalent fixation of the vesicular bilayer microstructure via polymerization can lead to enhanced stability of the vesicles and also adjusts the bilayer permeability.<sup>36,37</sup> Polymerization can be further categorized into “polymerization in”<sup>38–42</sup> and “polymerization of” vesicles. In the case of “polymerization in” catanionic vesicles, hydrophobic monomers (styrene) swell the vesicle bilayers and are subsequently polymerized.<sup>43–48</sup> Dialysis is then carried out to remove the surfactant vesicle template to obtain hollow polymer nanospheres, which can only be redispersed in water with the aid of surfactant or after chemical modification (sulfonation).

Alternatively, we have reported that stabilization of catanionic vesicles can be readily accomplished employing a “polymerization of” approach.<sup>32</sup> Two polymerizable surfactants, methacryloyloxyundecyl trimethylammonium bromide (MUTB) and sodium 4-( $\omega$ -methacryloyloxyundecyl)oxy benzene sulfonate (MUBS), were synthesized. The formation and subsequent structural fixation of the catanionic vesicles via polymerization was evidenced by laser light scattering (LLS), cryo-transmission electro microscopy (cryo-TEM), and small angle neutron scattering (SANS). Unfortunately, the polymerizable anionic surfactant, MUBS, has a Krafft point of  $\sim 43$  °C. Thus these two surfactants need to be mixed at  $\sim 50$  °C to form catanionic vesicles before they can be polymerized in situ upon addition of a water-soluble free radical initiator. This temperature requirement makes kinetics studies of vesicle formation and breakdown impractical. The details of the kinetics of vesicle formation and breakdown are thus unclear.

Herein, we synthesized two polymerizable surfactants with low Krafft points ( $<5$  °C), namely, methacryloyloxyoctyl trimethylammonium bromide (MOTB) and sodium 4-( $\omega$ -methacryloyloxyoctyl)oxy benzene sulfonate (MOBS). Using a combination of stopped-flow light scattering, surface tensiometry, static and dynamic LLS, cryo-TEM, and <sup>1</sup>H NMR, we address the following three questions in this study: (1) the kinetics of catanionic vesicle formation from MOTB/MOBS; (2) the kinetics of vesicle breakdown upon dilution or addition of excess of MOTB; (3) the structural parameters of polymerized catanionic vesicles and their stability upon dilution with water or addition of excess MOTB.

## Experimental Section

**Materials.** 1,8-Octanediol and phenol-4-sulfonic acid sodium dehydrate were purchased from Fluka. The initiator, 2,2'-azobis-(2-methylpropionamide) dihydrochloride (V50) (Wako Pure Chemical Industries, Ltd), was recrystallized from methanol. Dowex 50W-X8(H) ion-exchange resin was obtained from Aldrich. Methacryloyl chloride was prepared by reacting methacrylic acid with phosphorus trichloride. 8-Bromo-1-octanol was prepared according to procedures reported by Babler et al.<sup>49</sup> The purity of the obtained 8-bromo-1-octanol was  $>99\%$  as evaluated by thin-layer chromatography (TLC) analysis. Sodium 4-(8-methacryloyloxyoctyl)-oxy benzene sulfonate (MOBS) were prepared as described previously.<sup>35</sup>

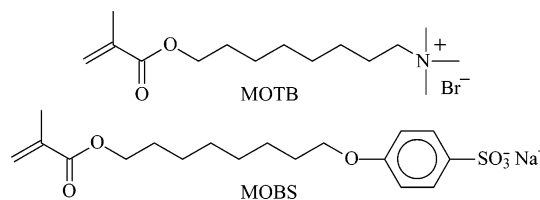


**Figure 1.** Chemical structures of methacryloyloxyoctyl trimethylammonium bromide (MOTB) and sodium 4-(8-methacryloyloxyoctyl)-oxy benzene sulfonate (MOBS).

**Preparation of MOTB.** MOTB was synthesized according to similar procedures reported previously.<sup>32</sup> Namely, 8-bromo-1-octanol (20 g, 0.095 mol) and 320 mL anhydrous THF were mixed in a flask at 0 °C under N<sub>2</sub>, followed by the addition of 10.8 mL (0.11 mol) methacryloyl chloride. The reaction mixture was bubbled with N<sub>2</sub> at room temperature for 2 h and then left stirring overnight. The unreacted methacryloyl chloride and solvent were removed under reduced pressure. The yellowish residue was dissolved in ethyl ether and washed with saturated sodium hydrogen carbonate solution until the aqueous layer was slightly basic (pH  $\sim 8.5$ ). After evaporation of the solvent, a viscous yellowish liquid of 8-bromooctyl methacrylate was obtained with a yield of 91%. MOTB with a yield of 75% was conveniently obtained by reacting 8-bromooctyl methacrylate with trimethylamine gas in diethyl ether at 0 °C following the procedure described by Michas et al.<sup>50</sup> The chemical structures of MOTB and MOBS are shown in Figure 1 and their purity was verified by <sup>1</sup>H NMR.

**Preparation of Vesicles, Phase Diagram Determination, and Polymerization.** Samples were prepared by first making stock solutions of MOBS and MOTB at the desired concentration in deionized water (Milli-Q) or D<sub>2</sub>O (Cambridge Isotopes). Vesicle samples were prepared by vortex-mixing the stock solutions for 10 s at the desired ratio and then storing the samples in a water bath thermostated at 25 °C.

For samples prepared for phase diagram measurement, dynamic light scattering, and surface tensiometry studies, several crystals of hydroquinone were added to the mixed solution to inhibit polymerization. Samples were thermostated at 25 °C for at least 3 days to reach final equilibrium, and then examined by eye to determine the number of phases. Single phases displaying Tyndall scattering were identified as possible vesicle phases, with the presence or absence of vesicle structures ultimately determined by the methods described below.

For the polymerization of vesicle samples, aqueous mixtures of two surfactants with molar ratios of MOTB/MOBS = 7/3 or 4/6 at a total concentration of 27 mM were prepared (27 mM MOTB is equal to 0.91 wt %, while 27 mM MOBS is equal to 1.06 wt %). The water-soluble initiator V50 was added (the molar ratio of (MOTB + MOBS)/V50 was fixed at 70/1), and the polymerization was conducted at 60 °C for 2 h.

**<sup>1</sup>H NMR Spectroscopy.** <sup>1</sup>H NMR measurements were performed at 25 °C using a Bruker AC300 NMR spectrometer (resonance frequency of 300 MHz for <sup>1</sup>H) operating in the Fourier transform mode.

**Laser Light Scattering (LLS).** A commercial spectrometer (ALV/DLS/SLS-5022F) equipped with a multi-tau digital time correlation (ALV5000) and a 22 mW UNIPHASE He–Ne laser ( $\lambda_0 = 632$  nm) as the light source was used. In static LLS, the weight-average molar mass ( $M_w$ ) and the radius of gyration ( $R_g$ ) of polymer chains in a dilute solution can be obtained from the

angular dependence of the excess absolute scattering intensity, known as Rayleigh ratio  $R_{vv}(q)$ , as

$$\frac{KC}{R_{vv}(q)} \approx \frac{1}{M_w} \left( 1 + \frac{1}{3} R_g^2 q^2 \right) + 2A_2C \quad (1)$$

where  $K = 4\pi^2 n^2 (dn/dC)^2 / (N_A \lambda_0^4)$  and  $q = (4\pi n / \lambda_0) \sin(\theta/2)$  with  $N_A$ ,  $dn/dC$ ,  $n$ , and  $\lambda_0$  being the Avogadro number, the specific refractive index increment, the solvent refractive index, and the wavelength of the laser light in a vacuum, respectively, and  $A_2$  is the second virial coefficient. The specific refractive index increment was determined by a precise differential refractometer at the same wavelength used for LLS studies. Strictly speaking,  $R_{vv}(q)$  should be  $R_{vu}(q)$  because of the absence of an analyzer before the detector. However, the depolarized scattering of the solution studied is insignificant so that  $R_{vu}(q) \sim R_{vv}(q)$ .<sup>51</sup>

In dynamic LLS, the Laplace inversion of each measured intensity–intensity–time correlation function  $G^{(2)}(q,t)$  in the self-beating mode can lead to a line-width distribution  $G(\Gamma)$ . For a pure diffusive relaxation,  $\Gamma$  is related to the translational diffusion coefficient  $D$  by  $(\Gamma/q^2)_{C \rightarrow 0, q \rightarrow 0} \rightarrow D$ , or further to the hydrodynamic radius  $R_h$  via the Stokes–Einstein equation,  $R_h = (k_B T / 6\pi\eta_0) / D$ , where  $k_B$ ,  $T$ , and  $\eta_0$  are the Boltzmann constant, the absolute temperature, and the solvent viscosity, respectively.

For catanionic vesicle samples before polymerization, dynamic LLS measurements revealed a slight increase of vesicular size over time within the first  $\sim 12$  h after mixing (Figure S1 in the Supporting Information). Thus the sizes of the final equilibrium catanionic vesicles were determined after thermally equilibrating the vesicular solutions at 25 °C for at least 3 days.

**Cryogenic Transmission Electron Microscopy (cryo-TEM).** Specimens for cryo-TEM were prepared in a controlled environment vitrification system (CEVS) described in detail by Bellare et al.<sup>52</sup> The sample vial was opened to withdraw the sample after the chamber contents were equilibrated at the desired temperature (25 °C) and relative humidity (95–99%). Specimens of the microstructured liquid were prepared by placing a drop of the sample on a lacey carbon film, supported by a copper grid (Ted Pella, Redding, CA) held by a pair of self-locking tweezers mounted on a spring-loaded shaft inside the environmental chamber. Thin liquid films of 50–500 nm cross sections were then formed by gently blotting away excess liquid on the grid by touching it with a filter paper. The liquid films were then vitrified by plunging the grid into liquid ethane, held at  $-180$  °C by a surrounding thermostated pool of liquid nitrogen. The grid was then transferred under liquid nitrogen onto the tip of a Gatan 626 cryo-transfer holder. Specimen was held at below  $-175$  °C and imaged at 120 kV in a Tecnai G2 12 transmission electron microscope. Images were recorded using a Gatan multiscan CCD camera at low dose.

**Surface Tensiometry.** Equilibrium surface tensions were measured using a JK99B tensiometer with a platinum plate. The measuring accuracy of the device as reported by the manufacturer is  $\pm 0.1$  mN/m. The surface tension of pure water (ca. 71 mN/m) was checked periodically between measurements. The reported surface tension at each concentration was the average of 3–5 measurements that were taken after allowing each of the solutions to equilibrate for  $\sim 1$  h in the instrument at a temperature of  $25.0 \pm 0.1$  °C.

**Stopped-flow Light Scattering.** Stopped-flow studies were carried out using a Bio-Logic SFM300/S stopped-flow instrument. The SFM-300/S is a 3-syringe (10 mL) instrument in which all step-motor-driven syringes (S1, S2, S3) can be operated independently to carry out single- to double-mixing. This device is attached to the MOS-250 spectrometer and the

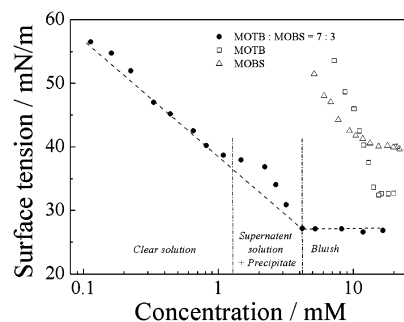


**Figure 2.** Surface tension of aqueous solutions of pure and mixed surfactants at 25 °C. For the mixture, the bulk mixing molar ratio is 7/3 MOTB to MOBS. The break in the surface tension curve represents the onset of aggregation (critical aggregation concentration, cac). Lines are shown to guide the eye.

collected kinetic data were fitted using the program Biokine (Bio-Logic). For light scattering detection, both the excitation and emission wavelengths were adjusted to 335 nm with 10 nm slits. The scattering angle was at 90°. Either a FC-08 or a FC-15 flow cell was used and the typical dead times were about 1.1 ms and 2.6 ms, respectively. The dynamic trace at each mixing ratio is averaged from 10 successive shots.

## Results and Discussion

**Surface Tensiometry and Phase Behavior.** Since MOTB and MOBS have Krafft points below 5 °C, surface tension measurements and phase map observations of pure surfactants and their mixtures were conveniently conducted at 25 °C. The critical micelle concentration (cmc) of pure MOTB surfactant monomer is 15.5 mM (0.52 wt %) and that of pure MOBS is  $\sim 13.4$  mM (0.53 wt %)<sup>32</sup> (see Figure 2). Mixtures of MOTB and MOBS exhibit a much lower surface tension value ( $\sim 25$  mN/m) than that of the two pure surfactant; meanwhile, the critical aggregation concentration (cac) of MOTB/MOBS mixtures at a molar ratio of 7/3 is significantly lower,  $\sim 4.2$  mM (0.15 wt %), than that of pure MOTB and MOBS surfactants.

Three different regions can be distinguished in the surface tension curve of the above mixture. The first region corresponds to monomer solution and occurs when the total surfactant concentration is less than 1.3 mM. The solution is clear and surface tension decreases steeply with total surfactant concentrations.<sup>53,54</sup> The second region occurs between 1.3 and 5.3 mM. In this region, precipitate appears after equilibration for several days and dynamic LLS of the supernatant solution measures large aggregates with intensity-averaged hydrodynamic diameters,  $D_h$ , of  $\sim 500$  nm. We did not attempt to check whether the supernatant solution contains vesicles or just irregular aggregates. It should be noted that the precipitate region is in the vicinity of the cac, so the cac of 4.2 mM measured by surface tension should correspond to the solubility of equimolar precipitate.<sup>5,55</sup> The third region is observed at a total surfactant concentration  $> 5.3$  mM. In this region, the surfactant mixture is homogeneous and bluish; the surface tension remains constant with increasing surfactant concentration. Thus, this region is ascribed as a vesicular phase region.

A partial phase map for mixtures of MOTB/MOBS/H<sub>2</sub>O at 25 °C in the water-rich corner (at total concentrations  $\leq 40$  mM,  $\sim 1.4$  wt %) is shown in Figure 3. Note that the phase rule does not allow a rigorous representation of a mixture of two salts and water at constant temperature on a triangular diagram. Samples close-to-equimolar ratio contain a vesicle phase in equilibrium with precipitate. On the MOTB-rich side, micelles form up to a mixing molar ratio of about MOBS/MOTB = 0.1.<sup>32</sup>

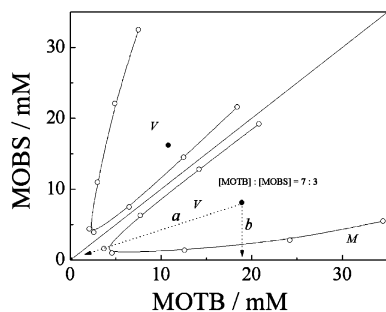


**Figure 3.** Partial phase map at 25 °C for mixtures of cationic surfactant methacryloyloxyoctyl trimethylammonium bromide (MOTB) and anionic surfactant sodium 4-( $\omega$ -methacryloyloxyoctyl)oxy benzene sulfonate (MOBS). Phase regions are: micelles (*M*), vesicles (*V*). Very small amounts of turbid wisps form in samples in the MOTB-rich vesicle lobe with compositions left of the dashed line. The ● mark the composition to be polymerized. Line *a* and line *b* follow the path of dilution and of adding excess of MOTB into the mixed surfactant solution, respectively.

Dynamic LLS measurements of solution mixtures in this region reveal very weak scattering intensities and intensity-averaged hydrodynamic diameter,  $D_h$ , of  $\sim 10$  nm. The small dimension and the fact that the solutions are clear suggest the presence of micellar structures. When additional MOBS is added, a bluish solution, which is a signature of the presence of vesicles, is observed.<sup>1,5,56</sup> Small amounts of turbid wisps form for those compositions in the MOTB-rich vesicle lobe at all mixing ratios investigated when the total concentration is less than  $\sim 5$  mM.

**Kinetics of Vesicle Formation.** Herein we use the stopped-flow device with a light-scattering detection to study the formation and breakdown of the cationic vesicles from MOTB and MOBS. It is known that for some systems, such as SOS/CTAB system, it takes several months to relax into the final equilibrium cationic vesicles,<sup>21,56,57</sup> whereas for other systems such as HDBS/CTAB, the vesicle formation process completes almost within minutes.<sup>20</sup> In the current case, it takes  $\sim 12$  h for the cationic vesicles to reach final equilibrium (Figure S1 in the Supporting Information). For kinetic studies, we only focus on the initial stages of the vesicle formation process, and the maximum experimental duration of stopped-flow measurements was  $\sim 1000$  s.

A typical dynamic curve of the vesicle formation process is shown in Figure 4, where the total surfactant concentration is 27 mM and the mixing ratio is MOTB/MOBS = 7/3. The time dependence of the scattering light intensity  $I_t$  can be converted to a normalized function, namely,  $(I_\infty - I_t)/I_\infty$  vs  $t$ , where  $I_\infty$  is the value of  $I_t$  at an infinitely long time. The fitting of the dynamic trace by a single exponential function is not good (Figure 4a), especially during the first tens of seconds, which

is the most interesting period to us since structural transition takes place during this initial stage. On the other hand, these dynamic curves could be well-fitted by a double exponential function (Figure 4b):

$$\frac{I_\infty - I_t}{I_\infty} = a_1 e^{-k_1 t} + a_2 e^{-k_2 t} \quad (2)$$

where  $a_1$  and  $a_2$  are the normalized amplitudes ( $a_2 = 1 - a_1$ ), and  $k_1$  and  $k_2$  are the relaxation constants. Characteristic relaxation times  $\tau$  can be obtained from  $\tau = 1/k$ , if the structural transitions are treated as first-order events.

Hatton et al. reported that the formation and growth of cationic vesicles following the mixing of two surfactant solutions should follow the sequence of 4 processes.<sup>21,23</sup> The first fast process ( $< 4$  ms) is associated with the formation of nonequilibrium mixed micelles. This was followed by the formation of loose or floppy bilayer structures through rearrangement of nonequilibrium mixed aggregates ( $\sim 4$  s), the formation of vesicle precursors ( $\sim 100$  s), and the formation of the final equilibrium vesicles ( $\sim 2000$  s).

The stopped-flow device used in this study has a dead time of  $\sim 2.6$  ms, so is likely that the relaxation process of the first fast step has completed within the dead time. Thus, the two relaxation times obtained in our case can be tentatively ascribed to  $\tau_{\text{floppy}}$ , the formation of “floppy bilayers”, and  $\tau_{\text{vesicle}}$ , the transition from floppy bilayers to vesicle precursors. Recall that since the maximum experimental duration of the stopped-flow measurements was  $\sim 1000$  s, the relaxation from vesicle precursors to the final equilibrium vesicles is not considered in this work.

The dependence of the kinetics of vesicle formation on the total surfactant concentrations has also been examined (Figure 5). Surfactant mixtures with total concentrations lower than 9 mM were not considered to avoid any interference from precipitate formation, which would take place at concentrations below 5.3 mM as discussed in previous section. From Figure 5, we can observe that scattering intensities after stopped-flow mixing of MOTB and MOBS at a molar ratio of MOTB/MOBS = 7/3 tend to stabilize after the first 200 s (Figure 5a). All the dynamic traces can be well-fitted with double exponential functions; the fitting results are shown in Figure 6. Over a range of total concentration 9–35 mM,  $\tau_{\text{floppy}}$  slightly increases from 12 to 16 s, while  $\tau_{\text{vesicle}}$  increases from 96 to 125 s. The corresponding normalized amplitudes,  $a_{\text{floppy}}$  and  $a_{\text{vesicle}}$ , are also plotted in Figure 6,  $a_{\text{floppy}}$  fluctuates around 0.4 and  $a_{\text{vesicle}}$  is  $\sim 0.4$  in the concentration range studied.

Figure 5b also shows the burst phase scattering intensities as a function of total surfactant concentration. The burst phase intensities are obtained by reading the value after extrapolating

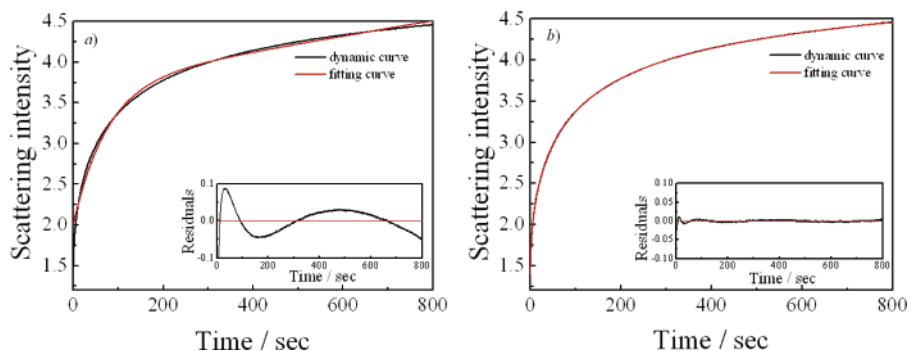


**Figure 4.** Typical time dependence of scattered light intensity of spontaneous vesicle formation. The dynamic curve is fitted by (a) single, or (b) double exponential functions, respectively. The mixing molar ratio of MOTB/MOBS is 7/3 with a total concentration of 27 mM.

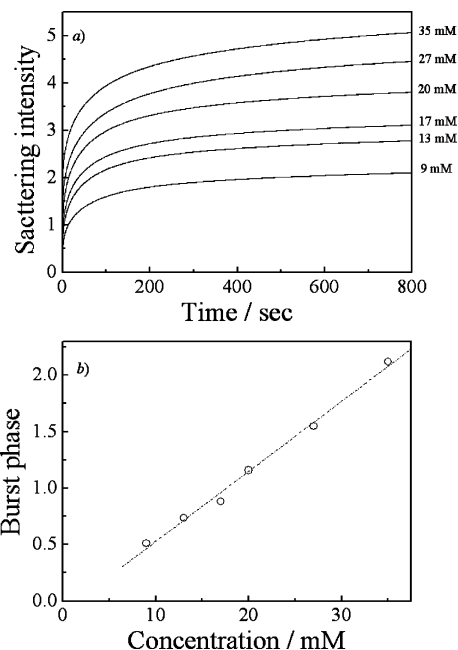


**Figure 5.** (a) Time dependence of the scattering light intensity after mixing MOTB with MOBS at different total surfactant concentrations. The mixing molar ratio is fixed at MOTB/MOBS = 7/3; (b) the burst phase scattering intensity as a function of total surfactant concentration.

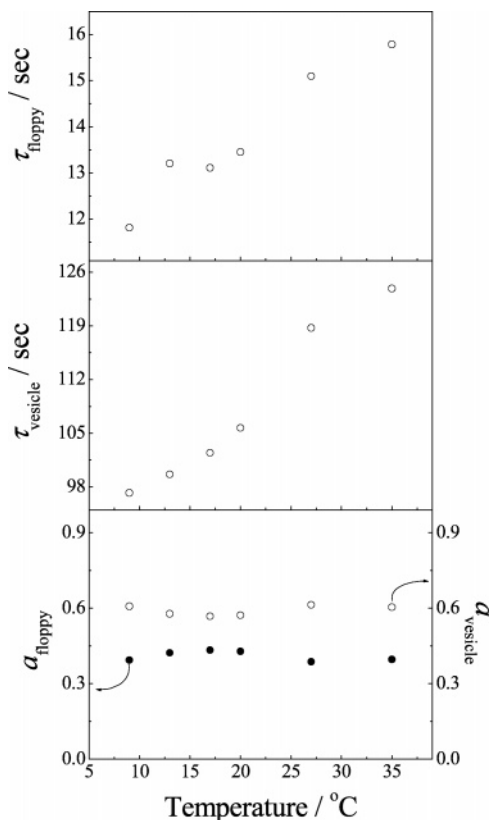


**Figure 6.** Relaxation times  $\tau_{\text{floppy}}$ ,  $\tau_{\text{vesicle}}$  and their corresponding normalized amplitudes,  $a_{\text{floppy}}$  and  $a_{\text{vesicle}}$ , as a function of total surfactant concentration. The mixing molar ratio is fixed at MOTB/MOBS = 7/3.

the double exponential fitting curve to  $-2.6$  ms, the dead time of the stopped flow device. Note that the burst phase scattering intensities increase linearly with total surfactant concentration, and the linear plot almost passes through the origin. These trends imply that the first fast process is simply associated with the formation of nonequilibrium mixed micelles or aggregates. The increase of total surfactant concentration only increases the

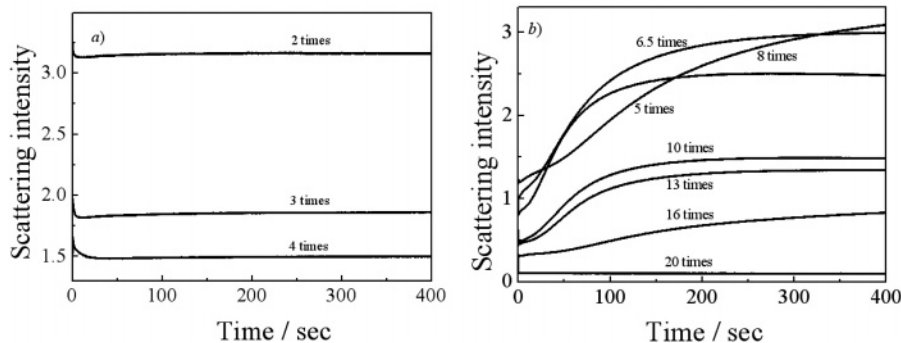
number density (number of aggregates per unit volume) of these initially formed aggregates.<sup>21</sup> There is no complex structural transition during the initial mixing (within a few milliseconds immediately after mixing). At intermediate total concentrations, such as at 20 mM, the concentration of MOTB and MOBS are both below their respective cmc values, charge equilibrium between the oppositely charged surfactants is expected to quickly take place.<sup>24</sup>

Gradzielski et al. have shown that initial mixed globular micelles quickly form and then dissolve with a time constant of  $\sim 0.5$ – $1$  s.<sup>24</sup> During and/or after the breakup of these mixed micelles, floppy bilayers form; this was followed by the formation of precursor unilamellar vesicles via a much slower process. Assuming a similar mechanism, the observed increase of  $\tau_{\text{floppy}}$  and  $\tau_{\text{vesicle}}$  with total surfactant concentration (Figure 6) provides strong evidence supporting that both the formation of floppy bilayers and precursor vesicles are dominated by unimer exchange between aggregates and unimers.<sup>13,14,25–28</sup> If these steps were dominated by fusion of initial floppy bilayers and small vesicles, respectively, both relaxation times,  $\tau_{\text{floppy}}$  and  $\tau_{\text{vesicle}}$ , would decrease with increasing total surfactant concentration, i.e., due to the faster kinetics of formation.

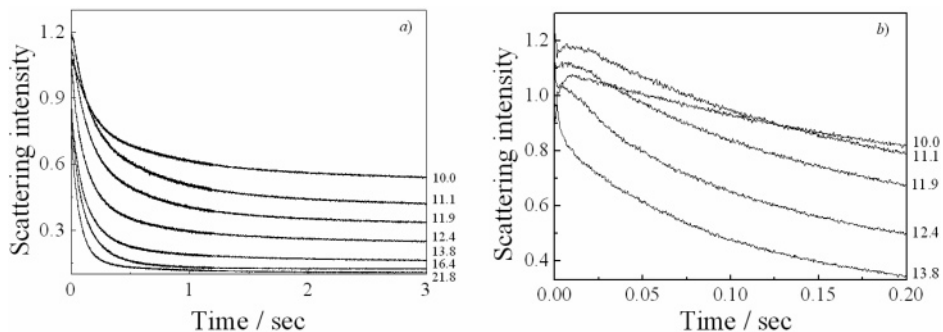
**Kinetics of Vesicle Breakdown.** Breakdown of catanionic vesicles can be induced by dilution with water or addition of excess single chain surfactant following path *a* or path *b* as indicated in Figure 3. It should be noted that the samples for the study of vesicle breakdown kinetics are subjected to  $\sim 15$  days storage, allowing them to reach final equilibrium. The studies of the kinetics of vesicle breakdown can lead to information such as the stability of vesicles, i.e., the average lifetime of catanionic vesicles. Polymerization of catanionic vesicle is expected to lead to permanent stable vesicular structures. A comparison between the average lifetime of catanionic vesicles and the propagation rate during free radical polymerization will lead to deeper understanding of the polymerization mechanism.

Figure 7 shows the dynamic traces after stopped-flow dilution of the unpolymerized catanionic vesicles at 27 mM with different amounts of water. With 2, 3, and 4 times of dilution, the scattering intensities exhibit an initial moderate decrease, which then flattens out within a few to tens of seconds (Figure 7a). The phase map shown in Figure 3 tells us that, even at 4 times of dilution, the final composition of the mixed surfactant solution still falls within the vesicle lobe. The initial slight decrease in light scattering intensities should reflect the change of vesicle size or size distributions. Separate dynamic LLS measurements of equilibrated cationic vesicles revealed that the change in vesicle size after 2, 3, or 4 times of dilution is negligible, but the size distributions broaden slightly. This suggests that slight decrease of scattering intensities should be ascribed to the change of size distributions upon dilution. Single-exponential fitting of the dynamic traces obtained from 4 times of dilution give a characteristic relaxation time of  $\sim 6$  s, whereas characteristic relaxation times of  $\sim 1.5$  s are obtained for that from 2 or 3 times of dilution.

When 5–16 times dilutions are conducted, an unexpected increase of scattering light intensities is observed (Figure 7b). A combination of data shown in Figure 2 and Figure 3 tells us that, throughout this range of dilutions, the resulting solution falls into the two phase region, i.e., precipitate plus supernatant solution. Disruption of the vesicles is expected to take place during dilution, further aggregation leads to precipitate formation after long storage time.



**Figure 7.** Time dependences of the scattering light intensities of unpolymerized catanionic vesicles immediately after different times of dilution with water. The molar ratio of MOTB/MOBS in the original solution is 7/3 with a total concentration of 27 mM.



**Figure 8.** Time dependence of the scattering light intensity after adding MOTB (18.9 mM) to the unpolymerized catanionic vesicle solutions at different final MOTB to MOBS molar ratios. The molar ratio of MOTB to MOBS in the original solution is 7:3 with a total concentration of 27 mM. The concentration of MOTB is always fixed at 18.9 mM.

When dilution is conducted for  $\geq 20$  times, no relaxation process is observed. The catanionic vesicles fall apart into unimers just within the “dead” time of the stopped-flow. The final surfactant mixtures fall into the clear solution region as shown in Figure 2.

Vesicle breakdown can also be achieved by mixing vesicle solutions with the addition of excess MOTB, i.e., path *b* in Figure 3.<sup>21,22</sup> The kinetic traces upon stopped-flow mixing catanionic vesicle solutions (27 mM total concentration, MOTB/MOBS = 7/3) with different amounts of MOTB (at a fixed MOTB concentration of 18.9 mM) are shown in Figure 8a. As reported by Robinson et al.,<sup>22</sup> the breakdown of catanionic vesicles upon addition of excess single chain surfactant should proceed in two steps. The first step involves the initial incorporation of single chain surfactant into the vesicle, followed by subsequent disintegration.

In this work, when the molar ratio MOTB/MOBS of the final surfactant mixture is less than 9, the final composition still lies in the vesicle lobe. Dynamic traces similar to those from less than 4 times dilution with water (Figure 7a) are obtained. In contrast, when the molar ratio of MOTB/MOBS in the final mixture is higher than 10, an abrupt decrease of scattering intensities is observed (Figure 8a). The final mixed solution is clear, which should be ascribed to mixed micelle formation. Edwards et al. have employed LLS and cryo-TEM to study the solubilization of lecithin vesicles by alkyl sulfate surfactant. At low concentrations of added surfactant, vesicle growth was observed; whereas at higher concentrations, a transformation into small globular lipid/surfactant mixture was observed. It seems that the breakdown of catanionic vesicles follows similar trends.<sup>7</sup>

However, a closer examination of the data in Figure 8a immediately after mixing (see Figure 8b) shows an initial slight increase of scattering intensities when the molar ratio of MOTB/MOBS in the final surfactant mixture is between 10 and 12.4.

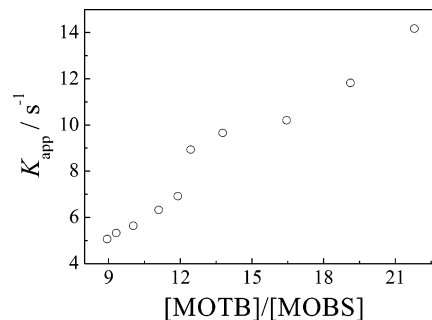


**Figure 9.** Breakdown of MOTB/MOBS vesicles on addition of different volumes of 18.9 mM MOTB solution. The molar ratio of MOTB to MOBS in original vesicle solutions is 7/3 with a total concentration of 27 mM.

The increase is complete within the first tens of milliseconds, which is followed by a quick decrease of the scattering intensities. The quick decrease of scattering intensities should be due to the vesicle breakdown into mixed micelles; the initial increase of scattering intensities within the first tens of milliseconds should be ascribed to the insertion of MOTB surfactant into the original vesicles, i.e., vesicle growth; the time scale is reasonable considering the translational diffusion rate constants of single chain surfactants. For MOTB/MOBS > 13, the process of MOTB insertion is expected to be much faster and the initial increase in scattering intensities is not observed anymore.

From Figure 8a, we can also tell that the higher the MOTB concentration (higher MOTB/MOBS ratio), the faster the breakdown of catanionic vesicles. The dynamic curves can be well-fitted with a single-exponential function, the obtained apparent rate constants are plotted against the molar ratio of MOTB/MOBS (Figure 9). The almost linear increase of the rate constant with increasing MOTB/MOBS molar ratio indicates that the driving force for vesicle breakdown is the addition of

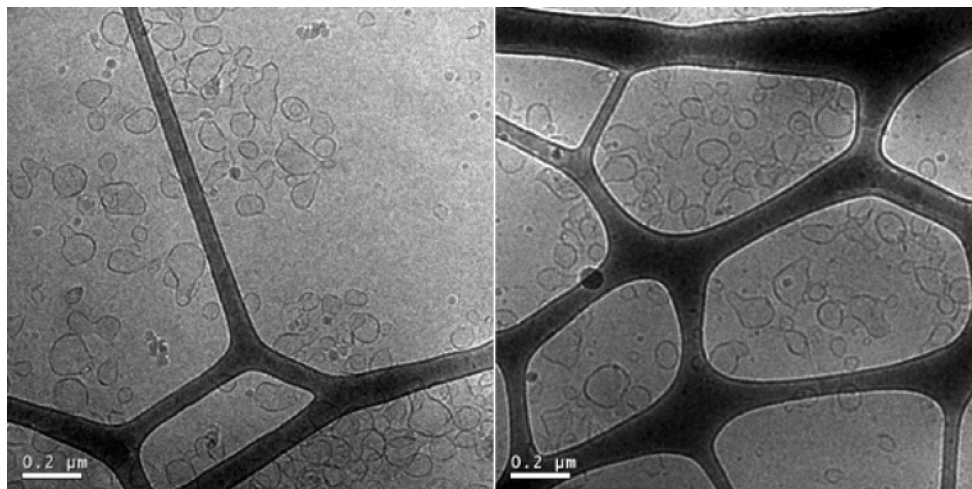


**Figure 10.** Cryo-TEM images of polymerized vesicles (the molar ratio of MOTB to MOBS is 7:3 with a total concentration of 27 mM) showing mostly spherical unilamellar vesicles with a few irregularly shaped vesicles due to vesicle fusion during the polymerization process.

excess of MOTB, which transforms the vesicle into mixed micelles.<sup>22</sup> It is quite understandable that the larger the driving force, the faster the transition from vesicles to mixed micelles. The breakdown of vesicles upon addition of excess single chain surfactant is quite fast (typical  $\tau_{\text{break}} \sim 0.1$  s), as compared with the vesicle formation process (tens or hundreds of seconds). This is in agreement with the results presented by Robinson et al.<sup>22</sup>

**Characterization of Polymerized Catanionic Vesicles.** Free radical polymerization was carried out on aqueous mixtures of MOTB and MOBS at molar ratios of MOTB/MOBS = 7/3 or 4/6 and a total concentration of 27 mM (Figure 3).<sup>32</sup> During polymerization, the bluish color, which is characteristic of the presence of catanionic vesicles, is visually unchanged. The polymerization of the catanionic vesicles is evidenced by <sup>1</sup>H NMR spectra (Figure S2 in the Supporting Information). The signals at  $\delta = 1.7$  ppm ( $\text{CH}_3$  on the methacrylate group of both surfactant monomers) and  $\delta = 5.2\text{--}5.9$  ppm ( $\text{CH}_2$  on the double bond) can be seen clearly for the unpolymerized vesicles. It is natural that the signal intensities for the methacrylate group appear weak and broad since this group is buried inside the hydrophobic vesicle bilayer. After polymerization for 2 h at 60 °C, all the signals characteristic of the unsaturated double bonds have disappeared, indicating complete polymerization of these groups. The resulted vesicle solutions are stable even after long storage (>6 months).

For aqueous mixtures of MOTB and MOBS at a molar ratio of MOTB/MOBS = 7/3, dynamic LLS measured an intensity-averaged hydrodynamic radius,  $R_h$ , of  $\sim 73$  and 74 nm for the vesicles before and after polymerization, respectively. Figure S3 in the Supporting Information reveals that the vesicle size does not change over  $\sim 400$  times of dilution (from 27 to 0.07 mM), which is far below the cac of the unpolymerized mixed surfactant solutions and the respective cmc values of two pure surfactants. Thus the successful fixation of these vesicles is self-evident. For vesicles with a composition of MOTB/MOBS = 4/6 at a total concentration of 27 mM, dynamic LLS reveals  $R_h$  of 65 and 68 nm for the unpolymerized and polymerized catanionic vesicles, respectively.

Cryo-TEM images of the above polymerized catanionic vesicles are shown in Figure 10. Cryo-TEM allows direct morphological characterization of the vesicles. It provides for the direct visualization of structural changes in the vesicles due to polymerization. Unpolymerized vesicles have been previously shown to be unilamellar and predominantly spherical.<sup>32</sup> After

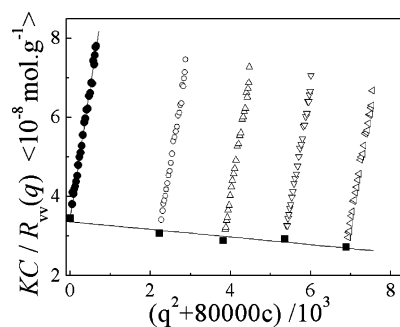


**Figure 11.** Zimm plot of polymerized vesicles prepared from aqueous surfactant mixtures of MOTB/MOBS = 7:3 with a total concentration of 27 mM. For the SLS measurement, a series of diluted polymerized vesicle samples with the concentrations ranging from  $2.78 \times 10^{-5}$  g mL<sup>-1</sup> to  $8.61 \times 10^{-5}$  g mL<sup>-1</sup> were used.

polymerization, unilamellar vesicles with diameters ranging from 100 to 200 nm are observed, along with the presence of some irregularly shaped unilamellar vesicles. The formation of these irregular unilamellar vesicles is probably due to polymerization-induced vesicle fusion,<sup>32</sup> although such structural transformations could be possibly induced by the introduction of ionic initiator as suggested by Hubert et al.<sup>58</sup> Water soluble initiators can act as hydrotropic salts, which are capable of altering the self-assembled nanostructures in surfactant solutions.<sup>59</sup>

Static LLS is then used to calculate the molar mass and the average radius of gyration,  $R_g$ , of the polymerized catanionic vesicles. Static LLS from the polymerized vesicles (Figure 11) yields a weight-average vesicle molar mass of approximately  $3.04 \times 10^7$  g mol<sup>-1</sup>. This value corresponds to approximately  $4.2 \times 10^4$  MOTB and  $1.8 \times 10^4$  MOBS molecules in each polymerized vesicle, based on the assumption that the molar ratio of MOTB to MOBS in the vesicles is the same as the bulk molar ratio. The  $R_g$  of the polymerized vesicles is  $\sim 76$  nm. This value leads to a  $R_g/R_h$  ratio of 1.03, which is close to the theoretical value of 1.0 for hollow nanospheres.<sup>25,27,60</sup> The above results confirm that vesicles are still the main structures after polymerization, although the process slightly disrupts the spherical vesicular microstructure.

**Stability of Polymerized Catanionic Vesicles.** Although there is no direct measurement the exchange rate between catanionic vesicles and monomers in the literature, it is generally accepted that there exists fast dynamic exchange between surfactant monomers and equilibrium catanionic vesicles, just in analogy with surfactant micellar solutions.<sup>13,14,25,27</sup> So the

treatment of the dynamics of surfactant micellar solutions are applied to the catanionic vesicle systems here. The nature of the dynamic exchange between vesicles and unimers can thus be described in terms of the average lifetime of vesicles, i.e., the time required for the association of surfactant monomers into the vesicles.<sup>61–64</sup> During polymerization, the mean lifetime of the unpolymerized vesicles ( $t_v$ ) can be calculated as<sup>61–63</sup>

$$t_v = N\tau_2 \quad (3)$$

where  $N$  is the average aggregation number in each unpolymerized vesicle, and  $\tau_2$  is related to the formation and breakdown of the vesicles, which can be estimated as  $\tau_{\text{break}} \sim 0.1$  s, as determined from Figure 9. If we take the average aggregation number determined for the polymerized vesicles as  $N$ , which is  $\sim 6 \times 10^4$  surfactant monomers,  $t_v$  is estimated to be  $\sim 6 \times 10^3$  s.

During polymerization of vesicles, the chain growth should mainly depend on the propagation time ( $t_p$ ) during which a monomer is added to the growing chain.  $t_p \approx (k_p M)^{-1}$ , where  $k_p \sim 1000$  ( $M$  s)<sup>-1</sup> for  $n$ -alkyl methacrylates with a degree of polymerization of 10 or higher and  $M$  is the monomer concentration.<sup>65,66</sup> For surfactant mixture at a total concentration of 27 mM,  $t_p \approx 4 \times 10^{-2}$  s at the initial stage of polymerization. This value is  $\sim 5$  orders of magnitude smaller than the average vesicle lifetime ( $\sim 6 \times 10^3$  s). This indicates that the microstructure of catanionic vesicles is rather static as compared to the rate of free radical propagation, although there is fast dynamic exchange between vesicles and monomers. The polymerization process partially resembles a typical microemulsion polymerization.<sup>47</sup> Free radicals decomposed from V50 first initiate surfactant monomer in the aqueous phase. These oligomeric chain radicals have chances to enter into the hydrophobic bilayer due to their amphiphilic nature. Once the oligomeric chain radicals enter into the vesicles, they will quickly polymerize and consume the methacrylate monomers completely. There is little chance of bi-radical termination because the likelihood of oligomeric chain radicals entering the same vesicles is extremely small, considering the number density of vesicles and the decomposition rate of initiator.

In previous reports of the polymerization of wormlike micelles,<sup>30,35</sup> the polymerized wormlike micelles were much longer in length than the unpolymerized wormlike micelles because the unimers in the aqueous phase can continuously participate into the polymerization. The microstructure of wormlike micelles is always open at both ends for insertion of surfactant monomers. Catanionic vesicles exist as closed bilayers entrapping a volume of aqueous phase inside; although there exist quick dynamic exchange between vesicles and surfactant monomers, polymerization will not considerably increase the size of vesicles.

We further employed stopped-flow light scattering to study the stability of polymerized catanionic vesicles upon dilution or addition of excess of MOTB. Figure S4 in the Supporting Information shows the dynamic traces of polymerized vesicles upon different times of dilution with deionized water. As opposed to that of the unpolymerized vesicles (Figure 7), we do not observe any relaxation process regardless of the times of dilutions.

The stability of the polymerized vesicles is further evidenced by stopped flow mixing polymerized vesicles with excess MOTB (Figure 12). In contrast to the unpolymerized vesicles (Figure 8), the scattering intensity of the polymerized vesicle solutions does not decrease upon addition of excess of MOTB even when the final MOTB/MOBS ratio goes as high as 20/1.

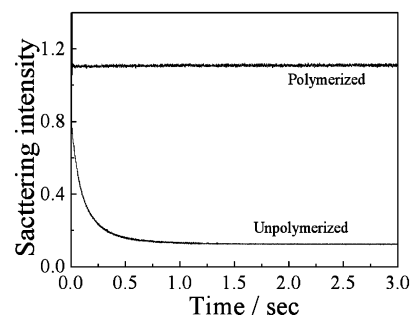


**Figure 12.** Time dependence of the scattering light intensities after adding excess MOTB (18.9 mM) to the unpolymerized and polymerized vesicle solutions. The molar ratio of MOTB to MOBS in initial vesicle solution is 7:3 with a total concentration of 27 mM, the final MOTB concentration was fixed at 18.9 mM and the ratio of MOTB/MOBS is 20/1.

These results further verify the structural integrity of the polymerized catanionic vesicles. After polymerization, the vesicle structures are infinitely stable to changes in solution conditions.

## Conclusion

Two polymerizable surfactants with low Krafft points, methacryloyloxyoctyl trimethylammonium bromide (MOTB) and sodium 4-(8-methacryloyloxyoctyl)oxy benzene sulfonate (MOBS), were synthesized. Catanionic vesicles form in mixed surfactant solutions. The kinetics of vesicle formation and breakdown are studied in detail by stopped-flow light scattering. Static and dynamic LLS, cryo-TEM and stopped-flow technique were further employed to characterize the structure and stability of the polymerized vesicles. The polymerization of catanionic vesicles can permanently capture the unilamellar vesicular microstructure. The structural integrity of polymerized vesicles can be well preserved under various perturbations, such as dilution or addition of excess single chain surfactants.

**Acknowledgment.** This work was supported by an Outstanding Youth Fund (50425310) and a key research grant (20534020) from the National Natural Scientific Foundation of China (NNSFC), the “Bai Ren” Project of the Chinese Academy of Sciences, and the Program for Changjiang Scholars and Innovative Research Team in University (PCSIRT).

**Supporting Information Available:** Four figures showing additional details of the experimental process. This material is available free of charge via the Internet at <http://pubs.acs.org>.

## References and Notes

- (1) Kaler, E. W.; Murthy, A. K.; Rodriguez, B. E.; Zasadzinski, J. A. *N. Science* **1989**, *245*, 1371–1374.
- (2) Hao, J. C.; Hoffmann, H. *Curr. Opin. Colloid Interface Sci.* **2004**, *9*, 279–293.
- (3) Svenson, S. *Curr. Opin. Colloid Interface Sci.* **2004**, *9*, 201–212.
- (4) Tondre, C.; Caillet, C. *Adv. Colloid Interface Sci.* **2001**, *93*, 115–134.
- (5) Kaler, E. W.; Herrington, K. L.; Murthy, A. K.; Zasadzinski, J. A. *N. J. Phys. Chem.* **1992**, *96*, 6698–6707.
- (6) Jung, H. T.; Coldren, B.; Zasadzinski, J. A.; Iampietro, D. J.; Kaler, E. W. *Proc. Natl. Acad. Sci. U.S.A.* **2001**, *98*, 1353–1357.
- (7) Silfvander, M.; Karlsson, G.; Edwards, K. *J. Colloid Interface Sci.* **1996**, *179*, 104–113.
- (8) Salkar, R. A.; Mukesh, D.; Samant, S. D.; Manohar, C. *Langmuir* **1998**, *14*, 3778–3782.
- (9) Mendes, E.; Menon, S. V. G. *Chem. Phys. Lett.* **1997**, *275*, 477–484.
- (10) Caillet, C.; Hebrant, M.; Tondre, C. *Langmuir* **2000**, *16*, 9099–9102.



- (11) Fischer, A.; Hebrant, M.; Tondre, C. *J. Colloid Interface Sci.* **2002**, *248*, 163–168.
- (12) Gradzielski, M. *J. Phys.: Condens. Matter* **2003**, *15*, R655–R697.
- (13) Gradzielski, M. *Curr. Opin. Colloid Interface Sci.* **2003**, *8*, 337–345.
- (14) Gradzielski, M. *Curr. Opin. Colloid Interface Sci.* **2004**, *9*, 256–263.
- (15) Soderman, O.; Herrington, K. L.; Kaler, E. W.; Miller, D. D. *Langmuir* **1997**, *13*, 5531–5538.
- (16) Mao, M.; Huang, J. B.; Zhu, B. Y.; Yin, H. Q.; Fu, H. L. *Langmuir* **2002**, *18*, 3380–3382.
- (17) Bujan, M.; Vdovic, N.; FilipovicVincekovic, N. *Colloids Surf., A* **1996**, *118*, 121–126.
- (18) Filipovic-Vincekovic, N.; Bujan, M.; Smit, I.; Tusek-Bozic, L.; Stefanic, I. *J. Colloid Interface Sci.* **1998**, *201*, 59–70.
- (19) Khan, A.; Marques, E. F. *Curr. Opin. Colloid Interface Sci.* **1999**, *4*, 402–410.
- (20) Xia, Y.; Goldmints, I.; Johnson, P. W.; Hatton, T. A.; Bose, A. *Langmuir* **2002**, *18*, 3822–3828.
- (21) O'Connor, A. J.; Hatton, T. A.; Bose, A. *Langmuir* **1997**, *13*, 6931–6940.
- (22) Bucak, S.; Robinson, B. H.; Fontana, A. *Langmuir* **2002**, *18*, 8288–8294.
- (23) Shioi, A.; Hatton, T. A. *Langmuir* **2002**, *18*, 7341–7348.
- (24) Schmolzer, S.; Grabner, D.; Gradzielski, M.; Narayanan, T. *Phys. Rev. Lett.* **2002**, *88*, 258301–1.
- (25) New, R. R. C. In *Liposomes: A Practical Approach*. IRL Press: Oxford, 1990; p 33–103.
- (26) Philippot, J. R.; Schuber, F. In *Liposomes as Tools in Basic Research and Industry*; CRC Press: Boca Raton, FL, 1994; p 276.
- (27) Evans, D. F.; Wennerstrom, H. *The Colloidal Domain: Where Physics, Chemistry, Biology, and Technology Meet*; VCH Publishers: New York, 1994.
- (28) Jonsson, B.; Lindman, B.; Holmberg, K.; Kronberg, B. *Surfactants and Polymers in Aqueous Solutions*; Wiley: New York, 1998.
- (29) Luo, S.; Xu, J.; Zhang, Y.; Liu, S.; Wu, C. *J. Phys. Chem. B* **2005**, *109*, 22159–22166.
- (30) Liu, S. Y.; Gonzalez, Y. I.; Danino, D.; Kaler, E. W. *Macromolecules* **2005**, *38*, 2482–2491.
- (31) Weaver, J. V. M.; Tang, Y. Q.; Liu, S. Y.; Iddon, P. D.; Grigg, R.; Billingham, N. C.; Armes, S. P.; Hunter, R.; Rannard, S. P. *Angew. Chem., Int. Ed.* **2004**, *43*, 1389–1392.
- (32) Liu, S. Y.; Gonzalez, Y. I.; Kaler, E. W. *Langmuir* **2003**, *19*, 10732–10738.
- (33) Liu, S. Y.; Weaver, J. V. M.; Tang, Y. Q.; Billingham, N. C.; Armes, S. P.; Tribe, K. *Macromolecules* **2002**, *35*, 6121–6131.
- (34) Liu, S. Y.; Armes, S. P. *J. Am. Chem. Soc.* **2001**, *123*, 9910–9911.
- (35) Zhu, Z. Y.; Gonzalez, Y. I.; Xu, H. X.; Kaler, E. W.; Liu, S. *Langmuir* **2006**, *22*, 949–955.
- (36) Gin, D. L.; Gu, W. Q.; Pindzola, B. A.; Zhou, W. J. *Acc. Chem. Res.* **2001**, *34*, 973–980.
- (37) O'Brien, D. F.; Armitage, B.; Benedicto, A.; Bennett, D. E.; Lamparski, H. G.; Lee, Y. S.; Srisiri, W.; Sisson, T. M. *Acc. Chem. Res.* **1998**, *31*, 861–868.
- (38) Jung, M.; den Ouden, I.; Montoya-Goni, A.; Hubert, D. H. W.; Frederik, P. M.; van Herk, A. M.; German, A. L. *Langmuir* **2000**, *16*, 4185–4195.
- (39) Jung, M.; Hubert, D. H. W.; van Herk, A. M.; German, A. L. *Macromolecular Symposia* **2000**, *151*, 393–398.
- (40) Jung, M.; Hubert, D. H. W.; van Veldhoven, E.; Frederik, P.; van Herk, A. M.; German, A. L. *Langmuir* **2000**, *16*, 3165–3174.
- (41) Hubert, D. H. W.; Jung, M.; German, A. L. *Adv. Mater.* **2000**, *12*, 1291–1294.
- (42) Zou, J. H.; Ye, X. D.; Shi, W. F. *Macromol. Rapid Commun.* **2005**, *26*, 1741–1745.
- (43) Morgan, J. D.; Johnson, C. A.; Kaler, E. W. *Langmuir* **1997**, *13*, 3, 6447–6451.
- (44) McKelvey, C. A.; Kaler, E. W.; Zasadzinski, J. A.; Coldren, B.; Jung, H. T. *Langmuir* **2000**, *16*, 8285–8290.
- (45) McKelvey, C. A.; Kaler, E. W. *J. Colloid Interface Sci.* **2002**, *245*, 68–74.
- (46) Hentze, H. P.; Raghavan, S. R.; McKelvey, C. A.; Kaler, E. W. *Langmuir* **2003**, *19*, 1069–1074.
- (47) Hentze, H. P.; Kaler, E. W. *Curr. Opin. Colloid Interface Sci.* **2003**, *8*, 164–178.
- (48) Hentze, H. P.; Co, C. C.; McKelvey, C. A.; Kaler, E. W. Templating vesicles, microemulsions, and lyotropic mesophases by organic polymerization processes. In *Colloid Chemistry I*; Springer-Verlag Berlin: Berlin, 2003; Vol. 226, pp 197–223.
- (49) Babler, J. H.; Invergo, B. J. *J. Org. Chem.* **1979**, *44*, 3723–3724.
- (50) Michas, J.; Paleos, C. M.; Dais, P. *Liq. Cryst. Cryst.* **1989**, *5*, 1737–1745.
- (51) Chu, B. *Laser Light Scattering: Basic Principles and Practice*, 2nd ed.; Academic Press: Boston, 1991.
- (52) Ballare, J. R.; Davis, H. T.; Scriven, L. E.; Talmon, Y. *J. Electron Microsc. Technol.* **1988**, *10*, 87–111.
- (53) Huang, J. B.; Zhao, G. X. *Colloid Polym. Sci.* **1995**, *273*, 156–164.
- (54) Villeneuve, M.; Kaneshina, S.; Imae, T.; Aratono, M. *Langmuir* **1999**, *15*, 2029–2036.
- (55) Yacilla, M. T.; Herrington, K. L.; Brasher, L. L.; Kaler, E. W.; Chiruvolu, S.; Zasadzinski, J. A. *J. Phys. Chem.* **1996**, *100*, 5874–5879.
- (56) Madani, H.; Kaler, E. W. *Langmuir* **1990**, *6*, 125–132.
- (57) Akisada, H.; Kuwahara, J.; Kunisaki, M.; Nishikawa, K.; Akagi, S.; Wada, M.; Kuwata, A.; Iwamoto, S. *Colloid Polym. Sci.* **2004**, *283*, 169–173.
- (58) Hubert, D. H. W.; Jung, M.; Frederik, P. M.; Bomans, P. H. H.; Meuldijk, J.; German, A. L. *Langmuir* **2000**, *16*, 8973–8979.
- (59) Gonzalez, Y. I.; Stjerndahl, M.; Danino, D.; Kaler, E. W. *Langmuir* **2004**, *20*, 7053–7063.
- (60) Brown, W. *Light Scattering, Principles and Development*; Clarendon Press: Oxford, England, 1996.
- (61) Aniansson, E. A. G.; Wall, S. N.; Almgren, M.; Hoffmann, H.; Kielmann, I.; Ulbricht, W.; Zana, R.; Lang, J.; Tondre, C. *J. Phys. Chem.* **1976**, *80*, 905–922.
- (62) Aniansson, G. E. A. *Prog. Colloid Polym. Sci.* **1985**, *70*, 2–5.
- (63) Cochin, D.; Zana, R.; Candau, F. *Macromolecules* **1993**, *26*, 5765–5771.
- (64) Lang, J.; Zana, R.; Bauer, R.; Hoffmann, H.; Ulbricht, W. *J. Phys. Chem.* **1975**, *79*, 276–283.
- (65) Hutchinson, R. A.; Beuermann, S.; Paquet, D. A.; McMinn, J. H. *Macromolecules* **1997**, *30*, 3490–3493.
- (66) Beuermann, S.; Paquet, D. A.; McMinn, J. H.; Hutchinson, R. A. *Macromolecules* **1997**, *30*, 194–197.